

Q_c and Q_s wave attenuation of South African earthquakes

Martin B. C. Brandt

Received: 16 July 2015 / Accepted: 2 November 2015 / Published online: 10 November 2015
© Springer Science+Business Media Dordrecht 2015

Abstract Quality factor Q , which describes the attenuation of seismic waves with distance, was determined for South Africa using data recorded by the South African National Seismograph Network. Because of an objective paucity of seismicity in South Africa and modernisation of the seismograph network only in 2007, I carried out a coda wave decay analysis on only 13 tectonic earthquakes and 7 mine-related events for the magnitude range $3.6 \leq M_L \leq 4.4$. Up to five seismograph stations were utilised to determine Q_c for frequencies at 2, 4, 8 and 16 Hz resulting in 84 individual measurements. The constants Q_0 and α were determined for the attenuation relation $Q_c(f) = Q_0 f^\alpha$. The result was $Q_0 = 396 \pm 29$ and $\alpha = 0.72 \pm 0.04$ for a lapse time of $1.9 * (t_s - t_0)$ (time from origin time t_0 to the start of coda analysis window is 1.9 times the S-travel time, t_s) and a coda window length of 80 s. This lapse time and coda window length were found to fit the most individual frequencies for a signal-to-noise ratio of at least 3 and a minimum absolute correlation coefficient for the envelope of 0.5. For a positive correlation coefficient, the envelope amplitude increases with time and Q_c was not calculated. The derived Q_c was verified using the spectral ratio method on a smaller data set consisting of nine earthquakes and one mine-related event recorded by up to four seismograph stations. Since the spectral ratio method requires absolute amplitudes in its calculations, site response tests were performed to

select four appropriate stations without soil amplification and/or signal distortion. The result obtained for Q_s was $Q_0 = 391 \pm 130$ and $\alpha = 0.60 \pm 0.16$, which agrees well with the coda Q_c result.

Keywords Quality factor · Q · Seismic wave attenuation · Coda · Amplitude ratio · South Africa

1 Introduction

Brandt and Saunders (unpublished work) recently undertook a preliminary study of an $M_w - M_L$ earthquake magnitude relation for South Africa using data recorded by the National Seismograph Network (Saunders et al. 2008) to develop a reliable moment magnitude scale for South Africa. Moment magnitudes are determined through spectral analysis of both P- and S-waves. However, the correct attenuation and geometrical spreading of seismic waves with distance is required (e.g. Havskov and Ottemöller 2010b) when undertaking a spectral analysis to calculate M_w . Since there are no appropriate regional attenuation studies available for South Africa, we obtained parameters from a similar tectonic domain, namely, Norway (Brandt and Saunders, unpublished work), although these cast a doubt on the reliability of the derived $M_w - M_L$ relation. In the broader region, Chow et al. (1980) analysed short-period Lg -waves from the then Rhodesian seismograph network to determine an average value for the specific quality factor Q for surface waves of 603 ± 50 for Zimbabwe with propagation paths along and across the East African Rift System; Hlatywayo and Midzi (1995)

M. B. C. Brandt (✉)
Seismology Unit, Council for Geoscience, Private Bag X112,
Pretoria 0001, South Africa
e-mail: mbrandt@geoscience.org.za

analysed *Lg*-waves using a single station to obtain an average value for Q of 650 for Zimbabwe with a low Q value of 350 for the Deka fault zone. My study has become feasible since the South African National Seismograph Network had been modernised in 2007—short-period sensors were replaced with broadband, and/or extended short-period seismometers and waveforms are presently recorded in miniSEED format. Data is transmitted to the analysis centre at 20 samples per second for continuous data and 100 samples per second for triggered data with the triggered data available to derive attenuation coefficient values (Saunders et al. 2008).

The amplitude decrease caused by attenuation can be described through the quality factor Q as had been proposed over 50 years ago (e.g. Havskov and Ottemöller 2010b)

$$A(f, t) = A_0 e^{\frac{-\pi f t}{2Q(f)}} \quad (1)$$

where A_0 is the initial amplitude, $A(t)$ the amplitude after the waves have travelled time t , f represents the frequency and $Q(f)$ is the general frequency dependent quality factor. Q has been observed to have strong regional variations in the lithosphere and a frequency dependence of the form (e.g. Kvamme and Havskov 1989; Kvamme et al. 1995; Malagnini et al. 2000)

$$Q(f) = Q_0 f^\alpha \quad (2)$$

when $f > 1$ Hz and $Q(f)$ is nearly constant for $0.1 \text{ Hz} < f < 1.0$ Hz (e.g. Stein and Wysession 2003). The frequency dependence is often found to be stronger with increasing tectonic activity and is thought to be related to the decrease of homogeneity in the crust (e.g. Kvamme and Havskov 1989). Q is also thought to be mostly constant along the ray path for local seismology observations, with the exception of the near-surface layers (1–3 km), which generally have a much lower Q than the rest of the path and tend to filter out high-frequency energy at frequencies greater than 10–20 Hz (e.g. Havskov and Ottemöller 2010b). The attenuation term in Eq. (1) may be separated into surface and deeper lithosphere

$$A(f, t) = A_0 e^{-\pi f \kappa} e^{\frac{-\pi f t}{2Q(f)}} \quad (3)$$

with κ as the near-surface attenuation. If, however, Q varies along the deeper path, the effect of different parts of the path must be accounted for. Rietbrock (2001) and Haberland and Rietbrock (2001) derived three-dimensional P-wave attenuation structures, and

Edwards et al. (2008) determined a depth-dependent Q structure. In my study, where Q is assumed to be mostly constant, the average Q along the path is determined.

Three routine methods are available to determine constant Q (Havskov and Ottemöller 2010b): (1) spectral modelling, where an observed spectrum can be modelled by trial and error, or better, by automatic fitting to determine the corner frequency f_0 , as well as κ , Q_0 and α ; (2) Q from coda waves that constitute the end of the seismic signal for local and regional events; and (3) two station methods; if seismic waves are recorded at different distances, the difference in amplitude at a given frequency is due to attenuation and geometrical spreading. A further development of the two station methods is the multi-station method where many events are recorded by multiple stations. This extended method can determine lateral variations in Q and local site amplifications if κ is assumed to be constant. In my study, I calculate the coda wave quality factor, Q_c , and verify the result against the two station S-wave quality factor, Q_s , which is determined for a data subset. I use the SEISAN earthquake analysis software (Havskov and Ottemöller 2010a) to determine Q_c with a coda decay analysis for various lapse times and coda window lengths. Q_s is calculated by means of spectral ratios for well-calibrated seismograph stations with minimal site amplification. Both methods only obtain $Q(f)$ and are unaffected by the near-surface attenuation, κ , if the contribution from the near-surface attenuation is small. This should be a good estimate since the geological basement in South Africa is of Archaean and Cambrian ages with few recent sedimentary deposits (e.g., Tankard et al. 1982) that can attenuate waves in the near surface. My analysis closely follows the routine data processing techniques prescribed by Havskov and Ottemöller (2010b). The resultant Q will be useful for the attenuation relation required by spectral analysis when calculating moment magnitude, $M_w(S)$, for S-waves with the seismograms recorded by the National Seismograph Network (Brandt and Saunders, unpublished work).

2 Methods

2.1 Coda decay analysis

The determination of Q from coda waves is a popular method since it requires only one station per earthquake and no calibration information for the seismograph.

Coda waves make up the end of the seismic signal for local and regional events and follow after the S and *Lg/Rg*-waves. Coda waves are thought to be S-to-S backscattered body waves which decrease in amplitude only due to attenuation (including scattering) and geometrical spreading (e.g. Kvamme and Havskov 1989; Havskov and Ottemöller 2010b). Coda decay analysis uses a single-scattering model to describe the attenuation of these waves (Aki and Chouet 1975). The coda amplitude decay may be expressed as

$$A(f, t) = t^{-\lambda} A_0 e^{-\pi f \kappa} e^{\frac{-\pi f t}{Q(f)}} \tag{4}$$

where dispersion parameter λ is 1 for body waves (scattered S-waves in the present scenario, e.g. Kvamme and Havskov 1989) and 0.5 for surface waves. A linear least squares analysis of the natural logarithm version of Eq. (4)

$$\ln(A(f, t)) + \lambda \ln(t) = \ln(A_0) - \pi f \kappa - \frac{t f \pi}{Q(f)} \tag{5}$$

can estimate the best fitting slope of an envelope of $\ln(A(f, t)) + \lambda \ln(t)$ as a function of t drawn through the positive amplitude values of one particular bandpass-filtered recording of Eq. (5). This gives a straight line with negative slope $\pi f / Q(f)$. Hence, $Q(f)$ can be determined without knowing the value of κ if the contribution from the near-surface attenuation is small. The average $Q(f)$ is obtained by inverting all the data sets simultaneously for one particular frequency or by averaging individual values (Kvamme and Havskov 1989).

Two routine methods are available to estimate coda Q : (1) calculating the envelope of the coda waves with an optimum fit to the peaks of the oscillating signals (e.g. Havskov and Ottemöller 2010b) and (2) calculating the envelope with a Hilbert transform (e.g. Lee and Sato 2006). A third, recently developed technique is a maximum likelihood method to simultaneously extract coda Q and the Nakagami-m parameter (Nakahara and Carcole 2010). In my study, I apply the simpler technique of fitting the peaks of the oscillating signal with an optimum envelope which is easy to implement and which yielded stable results. Events with a coda that has an adequate signal-to-noise ratio between 1 and 24 Hz were recorded by up to five broadband and/or extended short-period seismometers of the National Seismograph Network (Saunders et al. 2008), originating from 13 tectonic earthquakes and 7 mine-related events for the magnitude range $3.6 \leq M_L \leq 4.4$ that

spanned the period of February 2007 to December 2011 (Fig. 1). Figure 2a, b depicts typical seismic signals recorded by the seismograph stations located at Komaggas (KOMG) and Silverton, Tshwane (SLR) with their respective coda decay analyses. For the analyses, the start of the coda window is selected with a lapse time of $1.9 * (t_s - t_0)$ (time from origin time t_0 to the start of coda analysis window is 1.9 times the S-travel time, t_s) and a window length of 80 s. Coda Q is sensitive to the choice of parameters and the reason for selecting this specific lapse time and window length as well as the effect on the coda decay analyses when selecting different parameters will be investigated below. For each Q determination, the coda window signals are filtered with increasing centre frequencies 2, 4, 8 and 16 Hz and corresponding increasing bandwidths. This avoids ringing during the signal processing as it defines constant relative bandwidths that also ensure that an equal amount of energy is included into each band. The envelope is calculated with a running root mean square (RMS) average in a 5-s window. The signal-to-noise ratio is the ratio between the filtered RMS value at the end of the coda window and a 15-s noise window before the P phase—a minimum value of 3 is required to accept a filtered window for coda decay analysis. An absolute correlation coefficient of less than 0.5 for the fitted envelope also results in the rejection of a filtered coda window for analysis—see the 16 Hz window in Fig. 2b. For a positive correlation coefficient, the envelope amplitude increases with time and Q_c is not calculated. The estimated Q_c values show a significant increase with frequency, confirming the assumption of Q having the dependence defined in Eq. (2) that the coda waves sample different parts of the crust due to their different frequency contents (where the value for Q generally increases with depth) or that the geometrical spreading is frequency dependent.

With the dispersion parameter $\lambda=1$ (for scattered body waves) and using a fixed lapse time of $1.9 * (t_s - t_0)$ together with a window length of 80 s, the results of the coda decay analyses are shown in Table 1 for all the earthquakes and events at all the stations. Average Q_c is estimated from a number of events averaged for the specific frequency, whereas inverted Q_c is obtained by inverting all the data sets simultaneously for one particular frequency under the constrain that all the data sets must have the same Q_c . The results give a frequency dependence of the form $Q_c(f) = 396 f^{0.72}$ when the attenuation parameters are averaged.

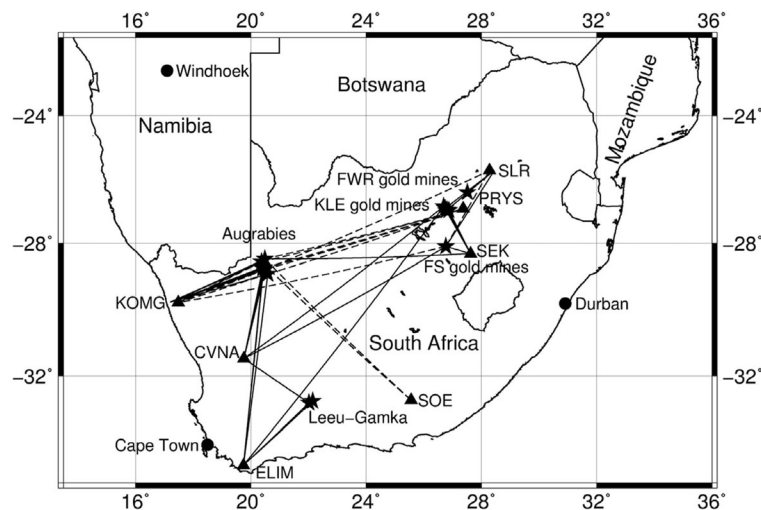


Fig. 1 Map of epicentres and recording stations of the data set. The coda decay analysis was carried out on up to five stations (triangles with station codes) that recorded coda waves travelling along ray paths (solid lines) having originated from 13 tectonic earthquakes and 7 mine-related events (stars). Spectral ratios were calculated at up to four stations (triangles with station codes) that recorded S-waves that travelled along ray paths (dashed lines)

The average lapse time with standard deviation is 161 ± 71 s.

Coda Q is sensitive to the choice of parameters, e.g. lapse time, window length, filter width, minimum signal-to-noise ratio and minimum correlation coefficient (e.g. Kvamme and Havskov 1989; Havskov and Ottemöller 2010b). Specifically, Q_0 and α vary for different lapse times (left panel, Fig. 3) and Q_0 mostly increases and α mostly decreases for longer windows (right panel, Fig. 3). If the lapse time is shorter than $1.8 \cdot (t_s - t_0)$, scattered S-waves that sampled the shallow crust are analysed rather than the coda waves from the deeper crust (e.g. Mukhopadhyay and Tyagi 2008). Coda waves from the shallow crust have a high signal-to-noise ratio and correlation coefficient, hence causing the number of coda windows accepted for analysis to increase drastically. A longer lapse time means that deeper, high Q crust is sampled by increasingly later-arriving coda waves. Thus, Q_0 increases and α decreases for lapse times longer than $2.0 \cdot (t_s - t_0)$, with these increases and decreases also seen for window lengths from 50 to 70 s (right panel, Fig. 3). The decreasing number of very long coda windows from 90 to 100 s most likely indicates amplitudes decreasing due to longer travel paths leading to a lower signal-to-noise ratio and correlation coefficient. However, Gusev (1995) argues that the effect of scattering decreases with depth in

originating from nine earthquakes and one mine-related event. Tectonic epicentres located near Leeu-Gamka and Augrabies; mine-related events located in the Free State (FS), Klerksdorp (KLE) and Far West Rand (FWR) gold mining areas. Stations are situated at Silverton, Tshwane (SLR), Parys (PRYS), Senekal (SEK), Calvinia (CVNA), Komaggas (KOMG), Elim (ELIM) and Somerset East (SOE)

the lithosphere and ascribes additional coda decay to intrinsic loss (heat, friction, etc. at increasing depth) which could also partially explain the decreasing number of very long coda windows. For my analyses, I selected a lapse time of $1.9 \cdot (t_s - t_0)$ and a window length of 80 s. These lapse time and window length were found to fit the most individual frequencies (Fig. 3) for a signal-to-noise ratio of at least 3 and hence sample the deeper crust without significant signal loss.

2.2 Spectral ratio

The spectral ratio method uses the ratio of signals of the same event recorded at two different seismograph stations (e.g. Campillo et al. 1985; Kvamme and Havskov 1989; Havskov and Ottemöller 2010b). The difference in amplitude at a given frequency is attributable to attenuation and geometrical spreading. Let the amplitudes recorded at station 1 be

$$A_1(f, t_1) = t_1^{-\beta} A_0 e^{-\pi f \kappa} e^{-\frac{\pi f t_1}{Q(f)}} \quad (6)$$

and ditto for $A_2(f, t_2)$ at station 2. If the amplitudes are observed at specific frequencies and travel times, if we assume a geometrical spreading i.e. set a value for β , and we assume that κ is constant and choose two stations along a great circle to avoid the effect of the radiation

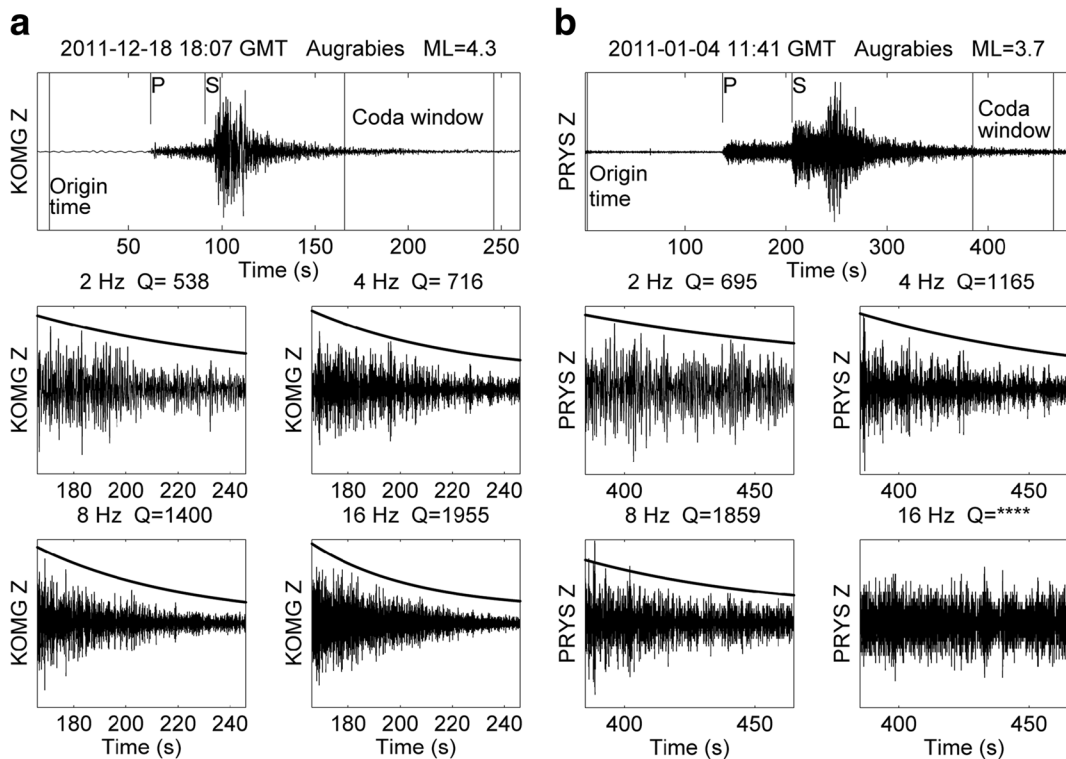


Fig. 2 **a** Example of a coda decay analysis at seismograph station KOMG to determine Q_c for an earthquake that occurred on December 18, 2011 at 18:07 GMT with epicentre near Augrabies, epicentral distance of 327 km and magnitude $M_L=4.3$. The *top trace* shows the seismogram with the origin time, P and S phases, and coda window. The *subsequent windows* show the coda Q analysis at frequencies 2, 4, 8 and 16 Hz with respective values for Q_c . **b** Example of a coda decay analysis at seismograph station

PRYS to determine Q_c for an earthquake that occurred on January 4, 2011 at 11:41 GMT with epicentre near Augrabies, epicentral distance of 707 km and magnitude $M_L=3.7$. The *top trace* shows the seismogram with the origin time, P and S phases, and coda window. The *subsequent windows* show the coda Q analysis at frequencies 2, 4, 8 and 16 Hz with respective values for Q_c . Note that for 16 Hz, the signal-to-noise ratio and correlation coefficient are too low to determine Q_c .

pattern, the resulting spectral ratio of the two seismic signals is

$$\frac{A_2(f, t_2)}{A_1(f, t_1)} = \left(\frac{t_2}{t_1}\right)^{-\beta} e^{-\frac{\pi f(t_2-t_1)}{Q(f)}} \tag{7}$$

Table 1 Number of coda windows accepted for analysis with inverted and average Q_c and α (with standard deviations) at the different frequencies. Average values at the different frequencies are averaged directly, whereas average Q_c is calculated by averaging $1/Q_c$ at the different frequencies to best fit the relation in Eq. (5)

Frequency (Hz)	2	4	8	16
Band (Hz)	1	2	4	8
Total no. of windows=84	16	26	27	15
Inverted $Q_c=394\pm 27$	610 \pm 87	1087 \pm 213	1681 \pm 293	2671 \pm 679
Average $Q_c=396\pm 29$	622 \pm 88	1129 \pm 230	1735 \pm 316	2874 \pm 846
Inverted α	0.70 \pm 0.04			
Average α	0.72 \pm 0.04			

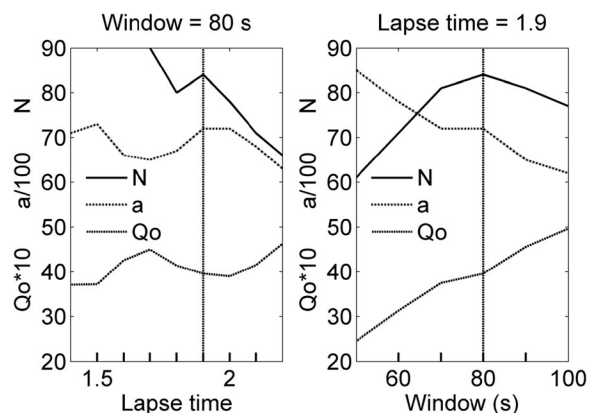


Fig. 3 Coda Q_0 , α and number of coda windows as a function of lapse time for a fixed window length of 80 s (*left panel*) and as a function of window length for a fixed lapse time of 1.9*(t_s-t_0) (*right panel*). Note that Q_0 is multiplied by a factor of 10 and α by a factor of 0.01

with $Q(f)$ the only unknown. Equation (7) may be linearized to calculate $Q(f)$ by taking the natural logarithm on both sides.

The spectral ratio method is critically dependent on the absolute amplitudes; hence, instruments must be precisely calibrated. Stations where soil and/or near-site amplifications or faulty recording equipment affecting the seismic signal should not be used. If, for example, station 2 is on soil or soft rock, the amplitude ratio in Eq. (7) includes the site-amplification factor in addition to the attenuation and geometrical spreading (e.g. Havskov and Ottemöller 2010b). I performed three tests to identify and reject stations affected by soil and/or near-site amplification, namely: (1) noise tests, (2) H/V spectral ratios and (3) amplification relative to a reference station. Noise tests are performed to identify unwanted signals from nearby man-made sources, faulty recording equipment, near-site scattering or distorted signals from poor sensor-to-bedrock coupling that could degenerate my analysis. Peterson (1993) developed seismic noise models to be used as a baseline for evaluating station site characteristics, equipment and noise sources. The standard Peterson low-noise (LNM) and high-noise models (HNM) represent average noise conditions at the stations of the Global Seismograph Network as a function of frequency with the highest probability power levels. Power density noise spectra at stations Koster (KSR), Gariep Dam (HVD) and KOMG are shown in the left panels of Fig. 4, with the LNM and HNM plotted as a reference. While all three spectra are within the limits of the LNM and HNM, noise power density at station HVD deviates from the smooth LNM between 2 and 10 Hz; this could indicate a local man-made noise source, faulty recording equipment or near-site scattering (which also shows up in the spectral ratio test below); hence, seismograms from this station were rejected for further analysis.

For the second test, I calculated Nakamura (1989) spectral ratios of the horizontal over the vertical channel for the same station: $H/V = A_H(f)/A_V(f)$. Since soil amplification mostly affects horizontal motion, an H/V ratio > 1 indicates a station with soil and/or near-site amplification (e.g. Fernandez and Brandt 2000). The average noise ratios with their standard deviations are shown in the right panels of Fig. 4. A significant ratio of ~ 3 to 5 between 1 and 3 Hz indicates soil amplification at station KSR, thus disqualifying these seismograms for my study. H/V ratios at station HVD show major

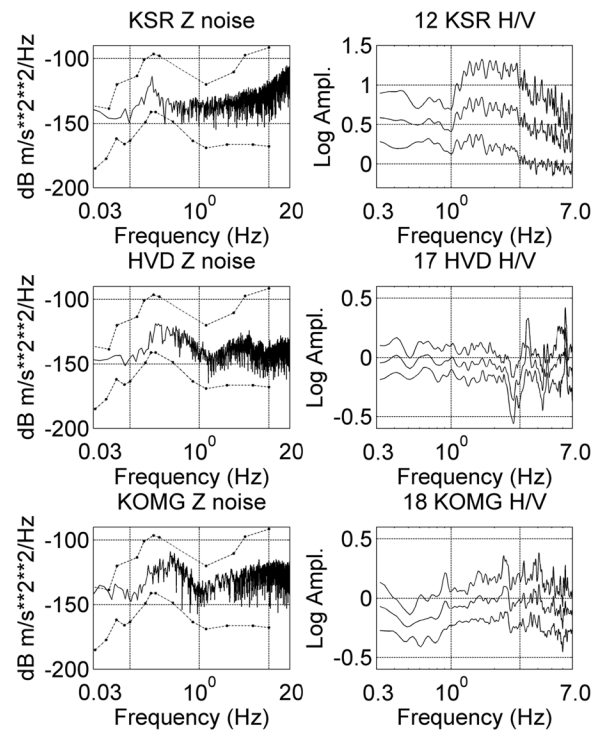


Fig. 4 Power density noise spectra (*solid lines*) at stations Koster (KSR), Gariep Dam (HVD) and KOMG are shown in the *left panels*. The standard Peterson (1993) low-noise model (LNM—*below*) and high-noise model (HNM—*above*) are plotted with *dash-dot lines* as a reference. In the *right panels*, average H/V spectral ratios with standard deviation (*below and above*) are shown for the same stations as in the left panels. *Numbers at the top left* indicate the number of H/V ratios used to derive the average

changes between 2 and 4 Hz, with a ratio varying between ~ 0.3 and 2, indicating near-site scattering or faulty recording equipment; thus, these seismograms were also rejected. The third test is discussed below.

For the spectral ratio analysis, I selected a subset of nine earthquakes and one mine-related event with seismograms recorded by up to four broadband and/or extended short period seismometers that had passed the noise and H/V ratio tests (Fig. 1). Since none of the two stations are on a great circle path, wave energy arrives at the two stations along different paths that could originate from different portions of the source radiation pattern. Since the pattern is not circular for earthquakes or mine-related events, the spectral ratio analysis can produce attenuation coefficient values that are either too low or too high, depending on the point of the radiation pattern on which the waves originate. The data set is too small to extend the analysis towards a multi-station method; hence, the effect of the source radiation on

different paths is cancelled by selecting several event-station distances and azimuths to obtain a stable average for Q_0 and α (e.g. Nuttli 1978, 1980). Figure 5a, b indicates typical seismic signals for the same earthquakes as those in Fig. 2a, b recorded by seismograph stations KOMG and PRYS, with their respective spectral ratio analyses. The coefficient for geometrical spreading, β , was fixed at 0.5 since all epicentral distances are more than 100 km and hypocentres are assumed to be shallow (Brandt 2014; Brandt and Saunders, unpublished work). S-waves are dominated by Lg -waves at distances greater than 100 km, and surface wave spreading is applied (Herrmann and Kijko 1980). A time window of 120 s starting at the S phase was used in all cases. Spectra were calculated for frequencies between 0.6 and 7 Hz. The low-frequency spectral ratio allowed me to perform a third test to

identify soil and/or near-site amplification: since Q is assumed to be nearly constant between $0.1 \text{ Hz} < f < 1 \text{ Hz}$, spectra with peaks and troughs for these low frequencies are rejected. Note, for example, the smooth constant ratio at low frequencies in Fig. 5b as opposed to the scenario depicted in Fig. 5a, which explains the rather low values for Q_0 and α for this event. Havskov and Ottemöller (2010b) recommend analysing spectra to as high a frequency as possible to obtain a stable fit to the data for Q_0 and α . However, Brandt and Saunders (unpublished work) completed spectral analyses on seismograms recorded by the national network and demonstrated that poor instrument calibrations that approximate the anti-alias filters at higher frequencies for most stations cause signal distortions around 10 Hz and this prevented me from including frequencies higher than 7 Hz.

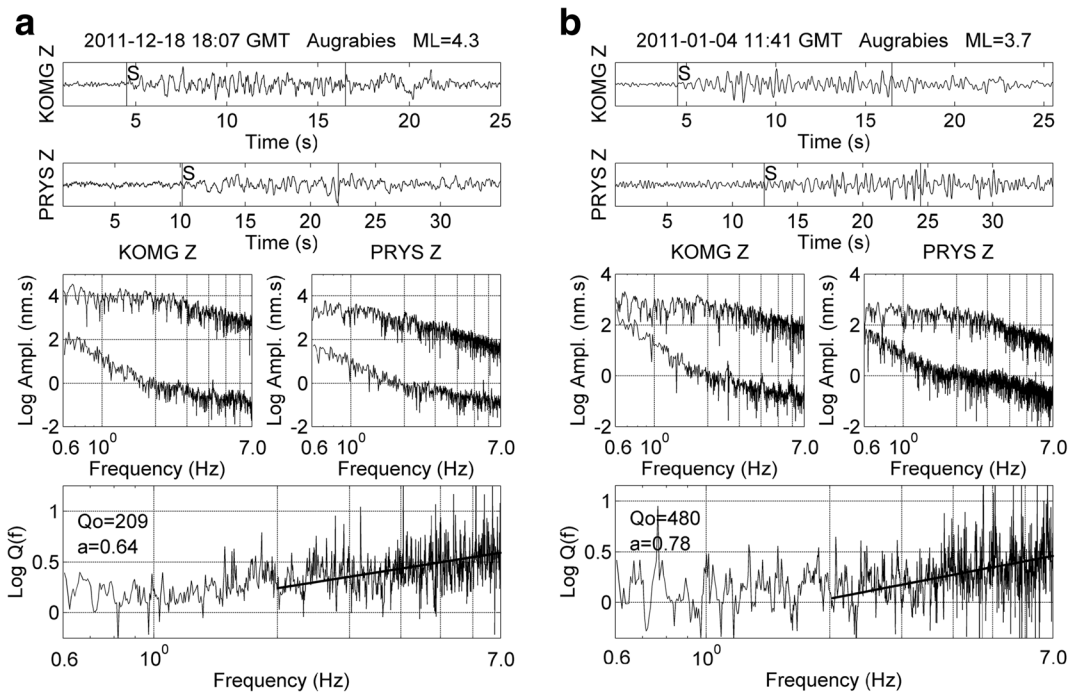


Fig. 5 a Example of a spectral ratio determined at seismograph stations KOMG and PRYS to obtain Q_s for an earthquake that occurred on December 18, 2011 at 18:07 GMT with epicentre near Augrabies, epicentral distance of 327 km and magnitude $M_L=4.3$. The top trace shows the seismogram with the S phase window selected for spectral analysis. The middle panels show the respective spectra for the signal (top) and noise (bottom). The bottom panel shows the log of the spectral ratio from which $Q(f)$ can be determined by means of Eq. (7). Numbers to the left refer to the least square fit of Q_0 and α to the ratio with Eq. (2) between 2 of 7 Hz. **b** Example of a spectral ratio determined at seismograph

stations KOMG and PRYS to obtain Q_s for an earthquake that occurred on January 4, 2011 at 11:41 GMT with epicentre near Augrabies, epicentral distance of 707 km and magnitude $M_L=3.7$. The top trace shows the seismogram with the S phase window selected for spectral analysis. The middle panels show the respective spectra for the signal (top) and noise (bottom). The bottom panel shows the log of the spectral ratio from which $Q(f)$ can be determined by means of Eq. (7). Numbers to the left refer to the least square fit of Q_0 and α to the ratio with Eq. (2) between 2 of 7 Hz

Averaged Q_S for my spectral ratio study is $Q_0=391\pm 130$ and $\alpha=0.60\pm 0.16$, which is in good agreement with the Q_c result in Table 1.

3 Discussion

The determination of Q from coda waves requires only one station per earthquake and no calibration information for the seismograph in comparison to the spectral ratio method which requires two stations and is critically dependent on the absolute amplitudes. However, coda Q is sensitive to the choice of parameters, specifically, the lapse time and window length, as high Q crust is sampled by increasingly later-arriving coda waves. Coda Q values are similar to Q_S provided that the same volume of lithosphere is sampled (Havskov and Ottemöller 2010b), which should be the case for this study since the earthquakes and events range in magnitude from 3.6 to 4.4 and cover a range of epicentral distances up to 924 km (Fig. 1). Coda waves from these events are expected to penetrate the crust to significant depths. Q_c was hence determined for the scattering crust which is thought to be also sampled by regional earthquake waves used to determine Q_S . My results for Q_c and Q_S are comparable to the value of $Q_0=400$ derived by Malagnini et al. (2000) for central Europe, which is slightly more than $Q_0=335$ determined by Zhu (2014) for the eastern China region and slightly less than that of the study by Kvamme et al. (1995). The latter study found $Q_0=470$ for Scandinavia. All three studies were for stable continental regions, and Brandt and Saunders, (unpublished work) surmised values of $Q_0=470$ and $\alpha=0.7$ for their first consideration of an M_w-M_L magnitude relation for South Africa. Malagnini et al. (2000) derived $\alpha=0.42$ for central Europe and Zhu (2014) $\alpha=0.45$ for eastern China, which differ significantly from my results, while Kvamme et al. (1995) obtained $\alpha=0.70$ for Scandinavia, exactly like this study for South Africa. My results differ significantly from studies for tectonically active regions (as may be expected), e.g. $Q_0=87$ and $\alpha=1.46$ for northern Iran (Motazedian 2006); $Q_0=40$ and $\alpha=0.45$ for the North Anatolian fault, Turkey (Akinci et al. 2001); $Q_0=127$ and $\alpha=0.96$ for the NW-Himalayas, India (Parvez et al. 2012); and $Q_0=80$ inside the San Andreas fault zone in California (Abercrombie 2000).

4 Conclusions

Quality factor, Q , was determined for South Africa using data recorded by the South African National Seismograph Network with the purpose of developing a reliable moment magnitude for South Africa. Values for constants $Q_0\approx 400$ and $\alpha\approx 0.7$ were obtained by means of a coda decay analysis and spectral ratio study; these values are comparable to those obtained in previous investigations for stable continental areas.

Acknowledgments This research was funded as part of the operation and data analysis of the South African National Seismograph Network. I wish to thank the Council for Geoscience for permission to publish my results. Zahn Nel undertook the language editing.

References

- Abercrombie RA (2000) Crustal attenuation and site effects at Parkfield, California. *J Geophys Res* 105:6277–6286
- Aki K, Chouet B (1975) Origin of coda waves: source, attenuation, and scattering effects. *J Geophys Res* 80:3322–3342
- Akinci A, Malagnini L, Herrmann RB, Pino NA, Scognamiglio L, Eyidogan H (2001) High-frequency ground motion in the Erzincan Region, Turkey: inferences from small earthquakes. *Bull Seismol Soc Am* 91:1446–1455
- Brandt MBC (2014) Focal depths of South African earthquakes and mine events. *J South Afr Inst Min Metall* 114:1–8
- Campillo M, Plantet J, Bouchon M (1985) Frequency-dependent attenuation in the crust beneath central France from Lg waves: data analysis and numerical modelling. *Bull Seismol Soc Am* 75:1395–1411
- Chow RAC, Fairhead JD, Henderson NB, Marshall PD (1980) Magnitude and Q determination in southern Africa using Lg wave amplitudes. *Geophys J R Astron Soc* 63:735–745
- Edwards B, Rietbrock A, Bommer JJ, Baptie B (2008) The acquisition of source, path, and site effects from microearthquake recordings using Q tomography: application to the United Kingdom. *Bull Seismol Soc Am* 98:1915–1935. doi:10.1785/0120070127
- Fernandez LM, Brandt MBC (2000) The reference spectral noise ratio method to evaluate the seismic response of a site. *Soil Dyn Earthq Eng* 20:381–388
- Gusev AA (1995) Vertical profile of turbidity and coda Q. *Geophys J Int* 123:665–672
- Haberland C, Rietbrock A (2001) Attenuation tomography in the western central Andes: a detailed insight into the structure of a magmatic arc. *J Geophys Res* 106:11,151–11,167
- Havskov J, Ottemöller L (2010a) SEISAN earthquake analysis software for Windows, Solaris, Linux and Macosx. Ver. 8.3. University of Bergen, Norway
- Havskov J, Ottemöller L (2010b) Routine data processing in earthquake seismology. Springer Science+Business Media. 347 pp. doi: 10.1007/978-90-481-8697-6

- Herrmann RB, Kijko A (1980) Short-period Lg magnitudes: instrument, attenuation and source effects. *Bull Seismol Soc Am* 73:1835–1850
- Hlatywayo DJ, Midzi V (1995) Determination of Lg-wave attenuation using single-station seismograms: a case study for Zimbabwe. *Geophys J Int* 123:291–296
- Kvamme LB, Havskov J (1989) Q in southern Norway. *Bull Seismol Soc Am* 79:1575–1588
- Kvamme LB, Hansen RA, Bungum H (1995) Seismic-source and wave-propagation effects of Lg waves in Scandinavia. *Geophys J Int* 120:525–536
- Lee WS, Sato H (2006) Power-law decay characteristics of coda envelopes revealed from the analysis of regional earthquakes. *Geophys Res Lett* 33:L07317. doi:[10.1029/2006GL025840](https://doi.org/10.1029/2006GL025840)
- Malagnini L, Herrmann RB, Koch K (2000) Regional ground-motion scaling in Central Europe. *Bull Seismol Soc Am* 90:1052–1061
- Motazedian D (2006) Region-specific key seismic parameters for earthquakes in Northern Iran. *Bull Seismol Soc Am* 96:1383–1395. doi:[10.1785/0120050162](https://doi.org/10.1785/0120050162)
- Mukhopadhyay S, Tyagi C (2008) Variation of intrinsic and scattering attenuation with depth in NW Himalayas. *Geophys J Int* 172:1055–1065
- Nakahara H, Carcole E (2010) Maximum-likelihood method for estimating coda Q and the Nakagami-m parameter. *Bull Seismol Soc Am* 100:3174–3182. doi:[10.1785/0120100030](https://doi.org/10.1785/0120100030)
- Nakamura Y (1989) A method for dynamic characteristics estimation of subsurface using microtremor on the ground surface. *Q R Railw Tech Res Inst* 30(1):25–33
- Nuttli OW (1978) A time-domain study of the attenuation of 10-Hz waves in the New Madrid seismic zone. *Bull Seismol Soc Am* 68:343–355
- Nuttli OW (1980) The excitation and attenuation of seismic crustal phases in Iran. *Bull Seismol Soc Am* 70:469–485
- Parvez IA, Yadav P, Nagaraj K (2012) Attenuation of P, S and coda waves in the NW-Himalayas, India. *Int J Geosci* 3:179–191
- Peterson J (1993) Observation and modelling of seismic background noise. US Geological Survey Technical Report No. 93-322, 94 pp
- Rietbrock A (2001) P wave attenuation structure in the fault area of the 1995 Kobe earthquake. *J Geophys Res* 106:4141–4154
- Saunders I, Brandt MBC, Steyn J, Roblin DL, Kijko A (2008) The South African National Seismograph Network. *Seismol Res Lett* 79:203–210. doi:[10.1785/gssrl.79.2.203](https://doi.org/10.1785/gssrl.79.2.203)
- Stein S, Wysession M (2003) Introduction to seismology, earthquakes and earth structure. Blackwell, 498 pp
- Tankard AJ, Jackson MPA, Eriksson KA, Hobday DK, Hunter DR, Minter WEL (1982) Crustal evolution of southern Africa. Springer, New York, 480 pp
- Zhu X-Y (2014) An inversion of Lg-wave attenuation and site response from seismic spectral ratios in the eastern China region. *Bull Seismol Soc Am* 104:1389–1399. doi:[10.1785/0120120359](https://doi.org/10.1785/0120120359)